Low-Symmetry, Mixed-Valent, μ-Oxo Technetium Complexes with Pyridine and Halide Ligands

M. J. Clarke,*† M. E. Kastner,‡ L. A. Podbielski,† P. H. Fackler,† J. Schreifels,§ G. Meinken,⊥ and S. C. Srivastava⊥

Contribution from the Department of Chemistry, Boston College, Chestnut Hill, Massachusetts 02167, Department of Chemistry, Bucknell University, Lewisburg, Pennsylvania 17837, Department of Chemistry, University of Missouri, St. Louis, Missouri 63121, and Medical Department, Brookhaven National Laboratory, Upton, New York 11973. *Received February 18, 1987*

Abstract: Dinuclear, asymmetric, and dissymmetric μ-oxo complexes of technetium, in which the two Tc atoms are in intimate electronic communication, have been synthesized and structurally characterized. The two types of complexes are isomers differing in their arrangement of equatorial ligands around each technetium, with the configurations being X_4 and $(pyridine)_4$ for the dissymmetric case and $X_3(pyr)$ and $(pyr)_3X$ for the asymmetric. A compound representative of the asymmetric complexes, $[(Pic)Cl_3(Pic)Tc–O–TcCl(Pic)_3Cl]$ (III), crystallizes in the monoclinic space group $P2_1/n$ with the following unit cell parameters: a = 12.421 Å, b = 15.471 Å, c = 18.764 Å, β = 93.174°, and Z = 4. The geometry is essentially octahedral around each Tc, with the equatorial ligands on the opposite metal atoms being staggered relative to one another. The average equatorial Tc(1)–N bond distance is 2.143 (4) Å, while the Tc(1)–Cl equatorial distance is 2.421 (2) Å and the axial Tc(1)–Cl distance is 2.407 (2) Å. On the second technetium the equatorial Tc(2)–N distance is 2.150 (4) Å, while the axial Tc(2)–N distance is somewhat longer at 2.188 (4) Å, due to a slight trans influence exerted by the bridging oxygen. The equatorial Tc–Cl bond distances range from 2.357 to 2.421 Å, apparently due to steric effects. The Tc(1)–O and Tc(2)–O bond lengths are 1.800 (3) and 1.837 (3) Å, respectively. Dissymmetric complexes of the type $[X(L)_4Tc–O–TcX_4L]$, where X = Cl or Br and L = pyridine, 4-picoline, and 3,5-lutidine, are also formed by spontaneous self-assembly but are immediately derived from the asymmetric species. In the solid state, both types of compounds exhibit a small magnetic moment ($\mu_{eff} \sim 0.9$–$1.3\ \beta$). EPR spectra of the dissymmetric complex, $[Cl(Pic)_4Tc–O–TcCl_4(Pic)]$ (I), whose structure has been previously reported, are consistent with an axial, binuclear species, containing splitting by two $I = {}^9/_2$ metal nuclei. Simulated EPR parameters for I are the following: $g_\parallel$ = 1.9275, $g_\perp$ = 1.997, $a_\parallel$ = 272.3 G, $a_\parallel'$ = 31.0 G, $a_\perp$ = 163.3 G, and $a_\perp'$ = 60.1 G. EPR of III suggest similar parameters in a rhombic spectrum. Three, relatively narrow, intervalence charge transfer bands occur around 10 000 cm^{-1} for both asymmetric and dissymetric species. Infrared Tc–O stretching frequencies are in the range 698–726 cm^{-1}, while Tc–Cl bands appear in the range 305–317 cm^{-1} and Tc–Br at 235–266 cm^{-1}. Cyclic voltammetry for both types of compounds typically revealed two separate and single-electron redox processes, which were sensitive to the ligands present. Comproportionation constants for I and III are 1.1×10^{25} and 4.0×10^{18}, indicating close electronic communication between the two technetium atoms in each complex. ESCA analysis for Tc 3d electrons revealed only a single peak for both technetiums in either I or III or the corresponding bromo analogues at 254.6 ± 0.2 eV, suggesting that the Tc ions in these complexes differ by no more than a single oxidation state. Tissue distributions of these complexes in animals are reported and discussed.

The chemistry of the synthetic element technetium has undergone rapid development in recent years, largely due to the widespread use of the metastable nuclide, ^{99m}Tc, in nuclear medicine.[1-3] Technetium complexes with heterocyclic imines, such as imidazole and pyridine, are useful model compounds for analogous complexes with nucleic acids and their constituent bases, histidine sites on proteins, and imine sites on some antibiotics. While Tc^V compounds with halides and chalcogenides usually contain $[Tc{\equiv}O]^{3+}$, with the other ligands arranged at the base of a square pyramid, complexes of Tc^V with nitrogen ligands generally yield *trans*-$[O_2L_4Tc]^+$, where L is a sterically unhindered nitrogen ligand.[4,5] Complexes of the type *trans*-$[O_2(pyr)_4Tc]^+$, where pyr = pyridine derivative, are readily formed on reacting common technetium starting materials with neat pyridine ligands at room temperature.[6] When pyridine derivatives with electron-withdrawing substituents are used in alcoholic solvents, compounds with the general formulation *trans*-$[O(RO)X_2(pyr)_2Tc]$ result, where X = Cl or Br and RO = CH_3O or CH_3CH_2O.[7]

Early Russian workers[8] had alluded to the appearance of a dark crystalline material on allowing *trans*-$[O_2(pyr)_4Tc]^+$ to stand in neat pyridine for extended periods. Indeed, if starting materials, such as $[OCl_4Tc]^-$, are heated to refluxing temperatures in neat pyridine solvents, the reactions proceed with *trans*-$[O_2(pyr)_4Tc]^+$ appearing; but continued heating produces a mixture of darkly colored, neutral complexes with the general formula $[OX_5(pyr)_5Tc_2]$. In the case of picoline, the final product has recently been shown to be a μ-oxo technetium complex, $[Cl(Pic)_4Tc–O–Tc(Pic)Cl_4]\cdot H_2O$,[9,10] which, owing to pinwheeling of the equatorial picolines in its more stable conformations, has only rotational symmetry and is dissymmetric. Subsequent work has uncovered asymmetric complexes, which are precursors of the dissymmetric species. The low symmetry of these complexes is unusual for class III mixed-valent compounds and unique for self-assembled μ-oxo species. In this work, the syntheses of both types of complexes with pyridine (Pyr), 4-picoline (Pic), and 3,5-lutidine (Lut) are reported and their spectroscopic characteristics described, together with a crystal and molecular structure determination of the asymmetric compound, $[Cl(Pic)_3ClTc–O–Tc(Pic)Cl_3(Pic)]$. Since

† Boston College.
‡ Bucknell University.
§ University of Missouri.
⊥ Brookhaven National Laboratory.

(1) Clarke, M. J.; Podbielski, L. *Coord. Chem. Rev.* **1987**, *78*, 253-331.
(2) Deutsch, E.; Buschong, W.; Glavan, K. A.; Elder, R. C.; Sodd, V. J.; Sholz, K. L.; Fortman, D. L.; Lukes, S. J., *Science* **1981**, *214*, 85-86 and references therein.
(3) Mazzi, U.; Nicolini, M. *Technetium in Chemistry and Nuclear Medicine*; Raven Press: New York, 1983.
(4) Kastner, M. E.; Lindsay, M. J.; Clarke, M. J. *Inorg. Chem.* **1982**, *21*, 2037-2040.
(5) Clarke, M. J.; Fackler, P. H. *Struct. Bonding (Berlin)* **1982**, *50*, 57-78.
(6) Kastner, M. E.; Fackler, P.; Deutsch, E.; Clarke, M. J. *Inorg. Chem.* **1984**, *23*, 4683-4688.
(7) Fackler, P.; Kastner, M. E.; Clarke, M. J. *Inorg. Chem.* **1984**, *23*, 3968-3972.
(8) Kuzina, A. F.; Oblova, A. A.; Spitsyn, V. I. *Russ. J. Inorg. Chem.* **1972**, *17*, 1377-1379.
(9) Kastner, M. E.; Fackler, P. H.; Podbielski, L.; Charkoudian, J.; Clarke, M. J. *Inorg. Chim. Acta* **1986**, *114*, L11-15.
(10) *aghij*-Pentachloro-μ-oxo-*bcdek*-pentakis(4-methylpyridine)ditechnetium monohydrate.

0002-7863/88/1510-1818$01.50/0

relatively small, neutral molecules are sometimes able to cross the blood–brain barrier, animal tissue distribution studies were also done in the hope that either type of complex might exhibit sufficient brain uptake to provide diagnostic brain images.

Experimental Section

Synthesis. The starting materials, $[(n\text{-}Bu)_4N][TcOX_4]$, were prepared from $(NH_4)TcO_4$ (Oak Ridge) by the method of Cotton (X = Cl)[11] and by a modification of the method of Preetz (X = Br),[12] which involved washing the final product with 0.1 M HBr. Compounds of the general types $[Cl(pyr)_4Tc\text{–}O\text{–}Tc(pyr)Cl_4]$ and $[Cl(pyr)_3ClTc\text{–}O\text{–}Tc(pyr)Cl_3(pyr)]$, where X = Cl or Br and pyr = pyridine, 4-methylpyridine, and 3,5-dimethylpyridine, were most often prepared by combining 0.25 mmol of $[(n\text{-}Bu)_4N][TcOX_4]$ or $[(n\text{-}Bu)_4N]_2[TcX_6]$ in 10 mL of the neat pyridine ligand in a 25-mL erlenmeyer. For the chloro series of compounds, yields seemed to be best starting with $[(n\text{-}Bu)_4N][TcOCl_4]$, while for the bromo complexes $[(n\text{-}Bu)_4N]_2[TcBr_6]$ was preferred. The use of underivatized pyridine appeared to favor the asymmetric complexes, while larger pyridine ligands, such as lutidine, gave relatively greater yields of the dissymmetric compounds. The solution was then heated to reflux with constant stirring, which resulted in a dark burgundy solution. The reaction was continued until TLC monitoring revealed an optimum amount of either the dissymmetric or asymmetric complex. After cooling, the mixture was transferred to a 25-mL round-bottom flask and rotary-evaporated to dryness. The residue was dissolved in a minimum amount of $CHCl_3$ and placed on a flash silica column (0.5 × 10 cm) and eluted with $CHCl_3$. The picoline compounds were also prepared from $(NH_4)TcO_4$ with added $(NH_4)X$ and $NaBH_4$ by a similar procedure.

The course of the reactions could be followed by thin-layer chromatography on silica plates developed with neat chloroform, or on reverse-phase C18 plates developed with 30% water in methanol. HPLC with 15-cm columns packed with 5-μm particles coated with octadecylsilane and eluted with 30% water in methanol also provided a rapid means of monitoring reactions. The compound $[Cl(Pic)_4Tc\text{–}O\text{–}Tc(Pic)Cl_4]$ eluted as the first band from silica and the third band on C18 systems. Highest quality crystals of this compound were most easily grown from chloroform solution with diffusion of diethyl ether to decrease solubility. The compound $[Cl(Pic)_3ClTc\text{–}O\text{–}Tc(Pic)Cl_3(Pic)]$ was isolated in the same fashion and crystallized from benzene solution with diffusion of diethyl ether.

Caution! All syntheses were performed with ^{99}Tc, which is a β-emitting isotope with a half-life of 2.15×10^5 y. (Only milligram quantities should be handled with the minimum shielding present under normal laboratory conditions.) Precautions for handling this material are described elsewhere.[1,5]

Compound Characterization. All elemental analyses (except for ^{99}Tc) were performed by the Stanford Microanalytical Laboratory, Stanford, CA, or the Berkley Microanalytical Laboratory, Berkley, CA. Technetium analyses were performed by dissolving known quantities of the compound in 8 mL of acetone and adding approximately 2 mL of a 30% solution of H_2O_2 to oxidize the metal to TcO_4^-. Calibration standards were similarly prepared by dissolving $(NH_4)TcO_4$ or $KTcO_4$, which had been recrystallized from 0.1 M ammonia with the addition of a few drops of H_2O_2, and then dried at 25 °C in a vacuum desiccator for 10 h. Aliquots of 25–125 mL were then combined with 10 mL of Fischer Scintiverse scintillation cocktail and Tc determinations made on an LKB-1217 scintillation counter. Counting was done for 60 s over a ^3H window (channels 8–110) with 10^4–10^5 counts usually being obtained for samples and standards. Unknown samples were determined with a linear least-squares fit to the standards. Elemental analyses are summarized in Table I.

Infrared spectra were taken on a Perkin-Elmer Model 599B grating spectrophotometer in CsI pellets. Resonance Raman spectra were obtained in dichloromethane at the MIT Regional Laser Facility on a Spex Ramalog spectrophotometer with an Ar laser line at 514.8 nm. Attempts to obtain solid-state Raman spectra invariably resulted in sample pyrolysis. UV–visible spectra were obtained on a Perkin-Elmer Model 575 equipped with a digital background corrector and a thermostated sample cell. Near-infrared spectra were taken on a Varian Model 2300 in $CHCl_3$, and intervalence charge transfer bands were resolved by a nonlinear regression analyses with a Lorentzian function to describe the bands.[13]

Electrochemical measurements were performed in 0.1 M tetraethylammonium perchlorate (TEAP) in DMF on a PAR-174A polarographic analyzer or on a versatile electrochemical apparatus constructed in this laboratory.[14] A platinum button working electrode, Ag/AgCl reference electrode, and platinum wire auxiliary electrode were used in all measurements. Reduction potentials were determined at the midpoint between the anodic and cathodic peaks of the cyclic voltammetric waveform (scanned at 125 mV/s) or at the peak of the differential pulse voltammetric waveform (scanned at 2 mV/s). Some chemically irreversible couples were determined at CV scans of 300 mV/s in order to minimize the subsequent chemical reaction. All potentials were internally referenced against the ferrocene couple (400 mV vs. NHE).[15] Conductance measurements were done in acetone with a Yellow Springs Instruments Model 32 conductance meter and a 1.0 mL conductance cell with a cell constant of 0.316 cm^{-1}.

Magnetic susceptibility studies were performed on a Cahn Model 7500 Electrobalance equipped with a 14502 G permanent magnet and a cryostat adapter to regulate temperature in the range −150 to 25 °C. ^1H NMR spectra were recorded on Varian FT-80A or 300 XL Fourier transform spectrometers. All spectra were recorded at room temperature with a spectral width of 2000 Hz. EPR spectra were taken of the pure solids and of the compounds dissolved in chloroform solution at −173, −50, and 24 °C on a Varian E-9 spectrometer.

Photoelectron spectra were recorded on a Varian IEE-15 spectrometer with a base pressure of 1×10^{-6} Torr. The spectrometer was equipped with an Al Kα X-ray source and operated at a constant pass energy of 100 eV. All spectra were referenced to the C(1s) spectrum, which has been shown to have a binding energy of 284.6 eV for hydrocarbons.[16] Replicate runs produced spectra with binding energies that were reproducible to within ±0.1 eV after referencing to the carbon peak. Samples were mounted by dusting them into cellophane tape. The oxygen peak for each compound was resolved into two peaks separated by about 2 eV on a Dupont 310 Curve Resolver.

Tissue Distributions. Two to ten millicuries of $[^{99m}TcO_4]^-$ were added to 1 mg of $(NH_4)[^{99}TcO_4]$ and the sample dried with a dry nitrogen stream in a small conical glass tube. The residue was dissolved in 0.5 mL of concentrated HCl and allowed to stand for 2 h before adding a nearly saturated aqueous solution of *n-tert*-butylammonium chloride dropwise until $[(n\text{-}C_4H_9)_4N][TcO_4]$ ceased to precipitate. After the starting compound was separated from the supernatant by centrifugation and washed twice with 0.1 M HCl, 250 μL of 4-picoline was added and the mixture refluxed for 0.5 h. Products were separated on a 0.5 cm × 10 cm silica gel column eluted with chloroform. After the chloroform

Table I. Elemental Analyses[a]

ligands L	ligands X	element	% calcd	% found $[XL_4TcOTcX_4L]\cdot H_2O$	% found $[XL_3XTcOTcLX_3L]\cdot H_2O$
Pyr	Cl	C	37.32	38.12	38.56
		H	3.38	3.17	3.18
		N	8.70	8.04	8.78
		Cl	22.0	23.0	22.11
		Tc	24.6	23.6	25.1
Pyr	Br	C	29.24	28.59	31.61
		H	2.65	2.36	2.73
		N	6.82	6.41	6.76
		Br	38.9	39.38	38.0
		Tc	19.3	19.2	19.0
Pic	Cl	C	40.19	40.43	41.48
		H	4.26	3.91	4.11
		N	8.01	8.16	7.92
		Cl	20.3	20.3	21.37
		Tc	22.6	22.9	22.5
Pic	Br	C	32.85	33.19	33.39
		H	3.40	3.35	3.35
		N	6.38	6.03	6.54
		Br	36.4	36.8	36.5
		Tc	18.0	17.9	18.2
Lut	Cl	C	44.49	45.03	46.75
		H	5.01	4.71	5.02
		N	7.41	7.49	7.46
		Cl	18.8	19.0	17.8
		Tc	20.9	20.0	21.0

[a] Pyr = pyridine, Pic = 4-methylpyridine (picoline), Lut = 3,5-dimethylpyridine (lutidine).

(11) Cotton, F. A.; Davison, A.; Day, V. W.; Gage, L. D.; Trop, H. S. *Inorg. Chem.* **1979**, *18*, 3024.
(12) Preetz, W.; Peters, G. *Z. Naturforsch.* **1980**, *35b*, 1355–1358.
(13) Fraser, B. D. B.; Suzuki, E. *Anal. Chem.* **1969**, *41*, 37–39.
(14) Clarke, M. J. *J. Am. Chem. Soc.* **1978**, *100*, 5068–5075.
(15) Gagnē, R. R.; Koval, C. A.; Lisensky, G. C. *Inorg. Chem.* **1980**, *19*, 2854–2855.
(16) Wagner, C. D.; Riggs, W. M.; Davis, L. E.; Muilenberg, G. E., Eds. *Handbook of X-ray Photoelectron Spectroscopy*; Perkin-Elmer Co.: Minneapolis, Minnesota, 1979.

Table II. Crystallographic Data for $[Cl(Pic)_3ClTc{-}O{-}Tc(Pic)Cl_3(Pic)]$

formula	$Tc_2O_1C_{30}H_{35}N_5Cl_5$
formula wt	856.9
cryst dimens	0.3 mm × 0.3 mm × 0.25 mm
color	dark reddish-brown, opaque
radiation source (Mo Kα)	λ = 0.71073 Å (graphite monochromator)
abs coef (μ), rel trans. factors	11.5 cm^{-1}, 0.915 to 1.0
diffractometer	CAD-4
space group	monoclinic, $P2_1/n$
cell constants	a = 12.421 (1) Å, b = 15.471 (1) Å, c = 18.764 (1) Å, β = 93.174 (5)°
cell vol	3600 (1) $Å^3$
Z (fw/unit cell)	4
d(calcd)	1.581 g/cm^3
total no. of observans	10,460
obsd reflcns[a]	7903
scan mode	θ–2θ
2θ range	4–60°
scan rate	2–5 deg/min
scan range	1.00 + 0.35 tan (θ)
no. of variables in least squares	388
$R = \sum(\|F_o\| - \|F_c\|)/\sum\|F_o\|$	0.054
$R_w = [\sum w(\|F_o\| - \|F_c\|)^2/\sum\|w(F_o)^2\|]^{1/2}$ [b]	0.038
goodness of fit = $[\sum w(\|F_o\| - \|F_c\|)^2/(N_{obsd} - N_{parameters})]^{1/2}$	2.8

[a] T = 24 (1) °C. Reflections with $F_o > 3\sigma(F_o)$ were retained as observed and used in the solution and refinement of the structure. Systematic absences were observed at: $h0l$, $h + l = 2n + 1$; $0k0$, $k = 2n + 1$. Three standard reflections were monitored with a limit of 0.2% variation. [b] Weighting scheme: $w = 4(F_o)^2[\sigma/(F_o)^2]^2$.

was removed with a nitrogen stream, the residues containing *trans*-$[O_2(Pic)_4Tc]^+$ and $[Cl(Pic)_4Tc{-}O{-}Tc(Pic)Cl_4]$ were each dissolved in 33% ethanol in 0.154 M NaCl, while $[Cl(Pic)_3ClTc{-}O{-}Tc(Pic)Cl_3(Pic)]$ was dissolved in 40% ethanol in 0.154 M NaCl.

Normal BNL mice weighing 26–35 g were slowly injected through their tail veins with 100 μL of these solutions, which contained approximately 1.7 μCi of ^{99m}Tc, over 30–60 s. The animals were sacrificed under an overdose of ether anesthesia at 5 min and 30 min. While all animals survived, they showed overt effects from the ethanol injections. Organs were excised and put into plastic counting vials and counted in a γ counter with a crystal (NaI) detector. The carcass was counted in three different tubes to maintain proper counting geometry. Three standards containing different volumes were determined to compensate for differing counting geometries, and the standard with the closest geometry to a given sample was used for comparison. Data were normalized to 25 g of body weight. Total recovery of radioactivity was determined for each animal, and the difference between recovered and injected radioactivity was attributed to excretion.

Structure Determination. Intensity data were collected on a CAD-4 automated diffractometer with background counts collected at the extremes of the scan for one-half the time of the scan. Four standard reflections were measured every 50 reflections during the course of the measurements with no change in intensity being observed over the course of the data collection. No absorption correction was applied. Crystallographic data are summarized in Table II.

The structure was solved with use of direct methods (MULTAN78)[17] to find the coordinates of the two technetium atoms, the bridging oxygen atom, and four chlorines.[18] Fourier methods[19] were used to find the locations of all other atoms. The structure was refined by full-matrix least-squares methods[20] and final bond distance and angles with estimated standard deviations were calculated.[21] The final model used anisotropic thermal parameters for all non-hydrogen atoms. The hydrogen atom positions were calculated (C–H distance 0.95 Å bisecting the C–C–C angle) and the isotropic temperature factors set at 1.0 $Å^2$ above the isotropic equivalent of the associated carbon. A final difference Fourier synthesis was judged free of significant features (highest peak 1 $e/Å^3$).

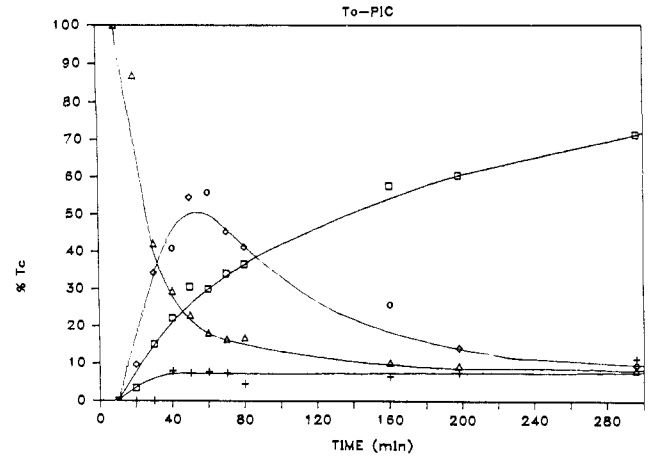

Figure 1. Kinetics of formation of compounds I, $[Cl(Pic)_4Tc{-}O{-}Tc(Pic)Cl_4]$, and III, $[Cl(Pic)_3ClTc{-}O{-}Tc(Pic)Cl_3(Pic)]$, and *trans*-$[O_2(Pic)_4Tc]^+$, where Pic = 4-methylpyridine (picoline): □, compound I $[Cl(Pic)_4Tc{-}O{-}Tc(Pic)Cl_4]$; +, compound II (*trans*-$[O_2(Pic)_4Tc]^+$), ◇, compound III ($[Cl(Pic)_3ClTc{-}O{-}Tc(Pic)Cl_3(Pic)][OCl_4Tc]^-$), △, starting material.

Results

Synthesis. Compounds with the general formulation $[X(L)_3XlTc{-}O{-}Tc(L)X_3(L)]$ and $[X(L)_4Tc{-}O{-}TcX_4L]\cdot H_2O$ were readily synthesized from almost any common technetium starting material including $(NH_4)_2TcX_6$, $[(n\text{-}Bu)_4N](TcOX_4)$, $[O_2(Pyr)_4Tc]Cl$, and *trans*-$[O(RO)Br_2(Pyr)_2Tc]$ by refluxing in the neat pyridine ligand. Preparation from $(NH_4)TcO_4$ was also possible in the presence of added chloride and a reductant. Formation of the μ-oxo species with chloride ligands was favored with $[(n\text{-}Bu)_4N](TcOCl_4)$ as a starting material, whereas yields of the corresponding bromo compounds were increased with $[(n\text{-}Bu)_4N]_2TcBr_6$. Running these reactions under argon did not significantly affect the product distributions or the rates of formation.

Figure 1 shows the change in reaction products and starting material as monitored by TLC for the reaction of $[(n\text{-}Bu)_4N](TcOCl_4)$ in refluxing picoline as a function of time. The starting material is sufficiently polar so that it remains at the origin. However, subsequent chromatography with more polar solvents, such as methanol, shows that the origin contains other radioactive products, so that the radioactivity at this point does not approach zero as a function of time. Compounds are labeled as a function of their TLC elution behavior. Dissymmetric compound I elutes first; *trans*-$[O_2(Pic)_4Tc]^+$ (II) elutes second, and the asymmetric III elutes third. In all cases monitored, the dissymmetric species is always the final product; however, the relative abundance is a function of the ligand used, with the more alkylated ligands favoring the dissymmetric complex. Following a typical 1 h reaction time essentially all of the recovered dinuclear product with lutidine was in the dissymmetric form, 80% of that with picoline and only 20% with pyridine.

These compounds are all insoluble in water and ether, partially soluble in methanol and ethanol, and quite soluble in common organic solvents, such as CCl_4, $CHCl_3$, CH_2Cl_2, acetone, DMF, benzene, toluene, acetonitrile, and DMSO. Conductance measurements in acetone revealed conductivities substantially below those of the comparison compound, sodium tetraphenylborate, and only slightly above those of the nonionic ferrocene or the solvent alone. Solutions of these complexes in ethanol passed quickly through both cation (Biorex 70 and Sephadex CM 25) and anion (Sephadex DEAE) ion exchange columns. However, if these solutions were allowed to remain on the column for longer than 20 s before elution, an increasing portion was observed to bind irreversibly to the column with time. Dissolution of these complexes in DMF did not alter the pH* of the solution and

(17) Main, P.; *Multan78*; Department of Physics, University of York, York, England.
(18) *International Tables for X-ray Crystallography*; Knyoch Press: Birmingham, England, 1974; Vol. 4.
(19) Hubbard, C. R.; Quicksall, C. O.; Jacobson, R. A. *The Fast Fourier Algorithm*; Ames Laboratory, Iowa State University: Ames, Iowa, 1971; Report 1s-2625.
(20) Lapp, R. L.; Jacobson, R. A. *ALLS, A Generalized Crystallographic Least Squares Program*, National Technical Information Service No. IS-4708 UC-4, Springfield, VA, 1979.
(21) ORFFE3, Crystallographic Function and Error Program Oak Ridge National Laboratory, Oak Ridge Tennessee, 37830.

Table III. UV-Vis Spectra of $[X(L)_4Tc-O-Tc(L)X_4]$ and $[X(L)_3XTc-O-Tc(L)X_3(L)]$ in $CHCl_3$[a]

ligands		$[X(L)_4Tc-O-Tc(L)X_4]$		$[X(L)_3XTc-O-Tc(L)X_3(L)]$	
L	X	λ_{max} (nm)	ϵ_{max} (10^{-4} M^{-1} cm^{-1})	λ_{max} (nm)	ϵ_{max} (10^{-4} M^{-1} cm^{-1})
Pyr	Cl	251	2.48	251	2.10
		362	1.23		
		408	2.14	399	1.67
		507	0.373	499	0.850
Pyr	Br	255	1.48	245	5.09
		279	1.35		
		378	0.45		
		430	0.832	423	1.39
		472	0.268		
		511	0.198	510	0.864
Pic	Cl	251	2.49	253	1.28
		360	1.32		
		406	2.30	398	1.55
		505	0.371	498	0.734
Pic	Br	250	2.20	248	2.12
				284 (sh)	1.50
		371	0.784		
				417	1.47
		478 (sh)	0.501		
		500	0.378	507	0.913
Lut	Cl	258	2.27	260	2.20
				292	0.501
		358	0.921		
		403	1.97	408	2.14
		506	0.306	507	0.373

[a] sh = shoulder.

attempts to titrate any ionizable hydrogens on these molecules with $(Et_4N)OH$ resulted in pH* curves identical with the solvent background.[22] Addition of these complexes to DMF solutions of $(Et_4N)OH$ also yielded no alteration in the pH*.

Spectra. The compounds appeared stable in the various organic solvents and exhibited no spectral change in ethanol over a period of hours from when they were freshly dissolved. The complexes obeyed Beer's law in ethanol, acetone, and chloroform over the concentration range 10^{-5} to 10^{-3} M and molar absorptivities in $CHCl_3$ are listed in Table III. The several overlaping bands found in the NIR region (see Figure 2), which are attributed to intervalence charge transfer (IVCT) transitions,[23] are listed in Table IV. Pertinent infrared assignments are summarized in Table V, with complete listings of all infrared bands available in the supplementary material. The asymmetric Tc–O–Tc stretching frequency occurs at somewhat higher energy than that observed in compounds of the type μ-O-$[OM(Et_2dtc)_2]_2$, where Et_2dtc = diethyldithiocarbamate and M = Tc (ν_{MOM} = 630 cm^{-1}) and Re (ν_{MOM} = 665 cm^{-1}).[24]

^1H NMR spectra exhibited resonances significantly broadened and shifted from those of the pure pyridine ligands, as expected for paramagnetic complexes. In the case of the dissymmetric lutidine complex with chloride ligands, the methyl protons on the axial ligands resonated at 9.2 ppm, while those on the equatorial ligands occurred at 3.5 ppm relative to TMS. For I the axial and equatorial methyl proton resonances were at 6.4 and 0 ppm, respectively. Compound III exhibited a number of ^1H NMR resonances (δ –0.3, 0.3, 0.9, 5.8, 8.2), perhaps owing to the presence of rotational isomers.

Photoelectron Spectroscopy. Photoelectron spectroscopy revealed the peak positions and widths for the elements in I to be very close to those in III (cf. Table VI). The small observable differences are in the range of reproducibility obtainable from repeated experiments with the same compound. In terms of peak widths, all elements scanned, with the exception of oxygen, produced spectra that were narrow and thus indicated either a single oxidation state or adjacent oxidation states for each. The chlorine spectrum is composed of an unresolved doublet corresponding to

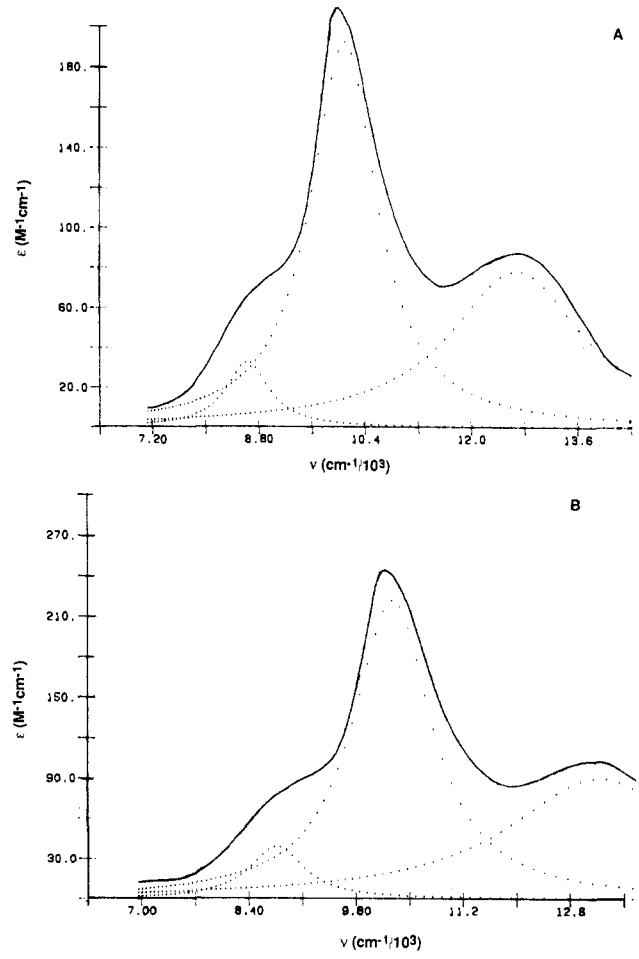

Figure 2. NIR spectrum of (A) $[Cl(Pic)_4Tc-O-Tc(Pic)Cl_4]$ and (B) $[Cl(Pic)_3ClTc-O-Tc(Pic)Cl_3(Pic)]$ in $CHCl_3$ at 23 °C. The solid line is the experimental spectrum, and dotted lines are the individual Lorentzian waveforms fitted to the experimental data.

the $2p_{1/2}$ and $2p_{3/2}$ electrons. The most intense of the two ($2p_{3/2}$) was chosen for binding energy determinations. The position of this peak in I with a binding energy of 197.5 eV was only slightly 0.5 eV) below its position in ionic chlorides. This indicates that the electron density around the chloride ions is approximately the same as in ionic chloride salts.[25] The position of the N(1s) peak at about 399 eV agrees well with those obtained for other ammines. The oxygen peak centered at 532.7 eV was broader than expected for oxygen bound to Tc. Fitting this peak as two overlapping bands gave 70% and 60% of the total area for I and III, respectively, to be located at 532.9 eV with the remainder being centered at 530.6 and 531.2 eV, respectively. The difference between the two low binding energy peaks can probably be attributed to a low signal-to-noise ratio. The low binding energy peak is slightly lower (0.5 to 1.2 eV) than has been observed for other technetium compounds[26] and is probably the bridging oxygen. The lower binding energy than for the oxygens in $[TcO_4]^-$ suggests a higher degree of electron density on the μ-oxo than on the pertechnetate oxygens. The oxygen peak at 532.9 eV is probably due to the water of hydration.[27-29]

The bromo analogues not only exhibit similar XPS binding energies for both technetiums in both compounds, but these en-

(22) Dowling, M. G.; Clarke, M. J. *Inorg. Chim. Acta* **1983**, *78*, 153–160.
(23) Creutz, C. A. *Prog. Inorg. Chem.* **1983**, *30*, 1–73.
(24) Trop, H. S. Ph.D. Thesis, 1979, MIT, p 109.
(25) Lawrence, S. S.; Schreifels, J. A., unpublished results.
(26) Wester, D. W.; Miller, F. W.; Dean, R. T.; Schreifels, J. A., submitted for publication.
(27) Roberts, M. W.; Wood, P. R. *J. Electron Spectrosc. Relat. Phenom.* **1977**, *11*, 431–437.
(28) Gimzewski, J. K.; Padalia, B. D.; Affrossman, S.; Watson, L. M.; Fabian, D. J. *Surf. Sci.* **1977**, *62*, 386–396.
(29) Fuggle, J. G.; Watson, L. M.; Fabian, D. J.; Affrossman, S. *Surf. Sci.* **1975**, *49*, 61–76.

Table IV. Intervalence Charge-Transfer Spectra of $[X(L)_4Tc-O-Tc(L)X_4]$ and $[X(L)_3XTc-O-Tc(L)X_3(L)]$ in $CHCl_3$[a]

ligands		$[X(L)_4Tc-O-Tc(L)X_4]$			$[X(L)_3XTc-O-Tc(L)X_3(L)]$		
L	X	ν_{max} (10^3 cm^{-1})	ϵ_{max} (M^{-1} cm^{-1})	$\Delta\nu_{1/2}$ (10^3 cm^{-1})	ν_{max} (10^3 cm^{-1})	ϵ_{max} (M^{-1} cm^{-1})	$\Delta\nu_{1/2}$ (10^3 cm^{-1})
Pic	Cl	8.62 (sh)	32	0.9	8.65 (sh)	39	0.9
		10.1	193	1.2	10.3	223	1.25
		12.7	79	2.5	13.0	90	2.81
Pic	Br	8.43	68	0.9			
		9.92	296	1.2	10.0	168	1.5
		12.3	120	2.8	11.9	118	4.1[b]

[a] sh = shoulder, $\Delta\nu_{1/2}$ = full band width at half-height, ϵ_{max} values are given for resolved peaks as indicated in the Experimental Section. [b] Evidence of additional peak, which could not be resolved, and decomposition of sample to yield a blue-colored species.

Table V. Infrared Stretching Frequencies of $[XL_4TcOTcX_4L]$ and $[XL_3XTcOTcLX_3L]$

ligands		stretching frequencies (cm^{-1})			
		$[XL_4Tc-O-TcLX_4]$		$[XL_3XTc-O-TcLX_3L]$	
L	X	Tc–O	Tc–X	Tc–O	Tc–X
Pyr	Cl	699	274, 317	702	242, 257, 290, 318, 343
Pyr	Br	698	244, 256	698	233, 240, 252
Pic	Cl	725	309, 322	726	258, 286, 322
Pic	Br	725	235, 310	724	235, 260, 310
Lut	Cl	702	270, 315		

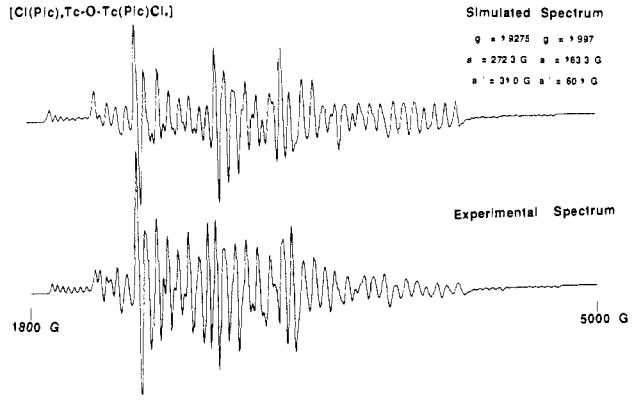

Figure 3. Simulated and experimental EPR spectra of $[Cl(Pic)_4Tc-O-Tc(Pic)Cl_4]$ in frozen $CHCl_3$ at −173 °C.

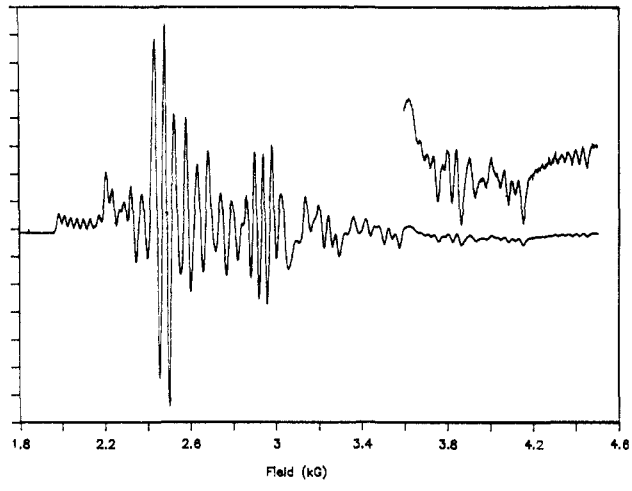

Figure 4. Experimental EPR spectra of $[Cl(Pic)_3ClTc-O-Tc(Pic)Cl_3-(Pic)]$ in frozen $CHCl_3$.

ergies are also similar to those of I and III. The carbon and nitrogen energies are also close to those in the chloro complexes. Similarly, the bromide ionization energy is essentially the same as that in ionic bromides (~68.5 eV). In contrast, the oxygen electrons are somewhat less tightly held.

Magnetic Properties. Magnetic susceptibility measurements taken over the range −150 to 25 °C (which showed apparent diamagnetism in small samples) yielded effective magnetic mo-

Table VI. ESCA Binding Energies (BE) and Full-Widths at Half-Maxima ($W_{1/2}$)

	$[Cl(L)_4TcOTc(L)Cl_4]$		$[Cl(L)_3ClTcOTc(L)Cl_3(L)]$		$[Br(L)_4TcOTc(L)Br_4]$		$[Br(L)_3BrTcOTc(L)Br_3(L)]$	
electron	BE(eV)	$W_{1/2}$ (eV)	BE (eV)	$W_{1/2}$ (eV)	BE (eV)	$W_{1/2}$ (eV)	BE (eV)	$W_{1/2}$ (eV)
Tc ($3d_{5/2}$)	254.6	2.6	254.4	2.6	254.7	2.4	254.7	2.9
Cl ($2p_{3/2}$)	197.5	2.9	197.3	2.9				
Br ($3d_{3/2,5/2}$)					68.2	2.5	67.9	2.3
N ($1s$)	398.9	1.7	399.2	1.9	399.4	1.9	399.2	2.2
O ($1s$)	532.7	3.3	532.6	3.4	532.1	3.3	531.6	3.1
C ($1s$)	284.6	2.5	284.6	2.5	284.6	2.4	284.6	2.1

Table VII. Formal Reduction Potentials of $[XL_4Tc-O-TcX_4L]$ and $[XL_3XTc-O-TXX_3L]$ in DMF

ligands		reduction potential (V)[a]							
		$[XL_4Tc-O-TcLX_4]$				$[XL_3XTc-O-TcLX_3L]$			
L	X	E_1	E_2	ΔE	K_{com}	E_1	E_2	ΔE	K_{com}
Pyr	Cl	0.864	−0.664[b]	1.528	1.3×10^{26}	0.602	−0.539[c]	1.159	6.4×10^{19}
Pyr	Br	0.737[d,e]	−0.515[f,d]	1.252	2.5×10^{21}	0.679	−0.298	0.977	4.9×10^{16}
Pic	Cl	0.74[g]	−0.74[h]	1.48	1.1×10^{25}	0.56	−0.54	1.10	4.0×10^{18}
Pic	Br	0.797[e]	−0.551[d,i]	1.348	1.1×10^{23}	0.612[j]	−0.354[k]	0.966	3.2×10^{16}
Lut	Cl	0.840[e]	−0.786[l]	1.626	6.1×10^{27}				

[a] Solutions adjusted to 0.1 M with $(Et_4N)ClO_4$ in DMF. Measurements were made by averaging the CV anodic and cathodic peak potentials. Scan rates are 125 mV/s, except for couples noted as irreversible, which were determined at 300 mV/s. Electrodes: WE, Pt-button; RE, Ag,AgCl; AE, Pt wire. [b] New anodic peak occurred around −325 mV after scanning over this potential. [c] Apparently reversible wave appears at 115 mV after scanning over this potential. [d] Chemically irreversible at 125 mV/s. [e] Additional broad irreversible oxidation peak grows in around 495 mV. [f] Additional irreversible oxidation peak grows in at −163 mV. [g] Apparently reversible peak grows in at 470 mV. [h] Irreversible peak grows in at −380 mV. [i] Additional irreversible oxidation peak grows in at −283 mV. [j] Additional irreversible couple at 1.0 V. [k] Apparently reversible couple grows in at −1.06 V. [l] Additional irreversible oxidation peak grows in at −438 mV.

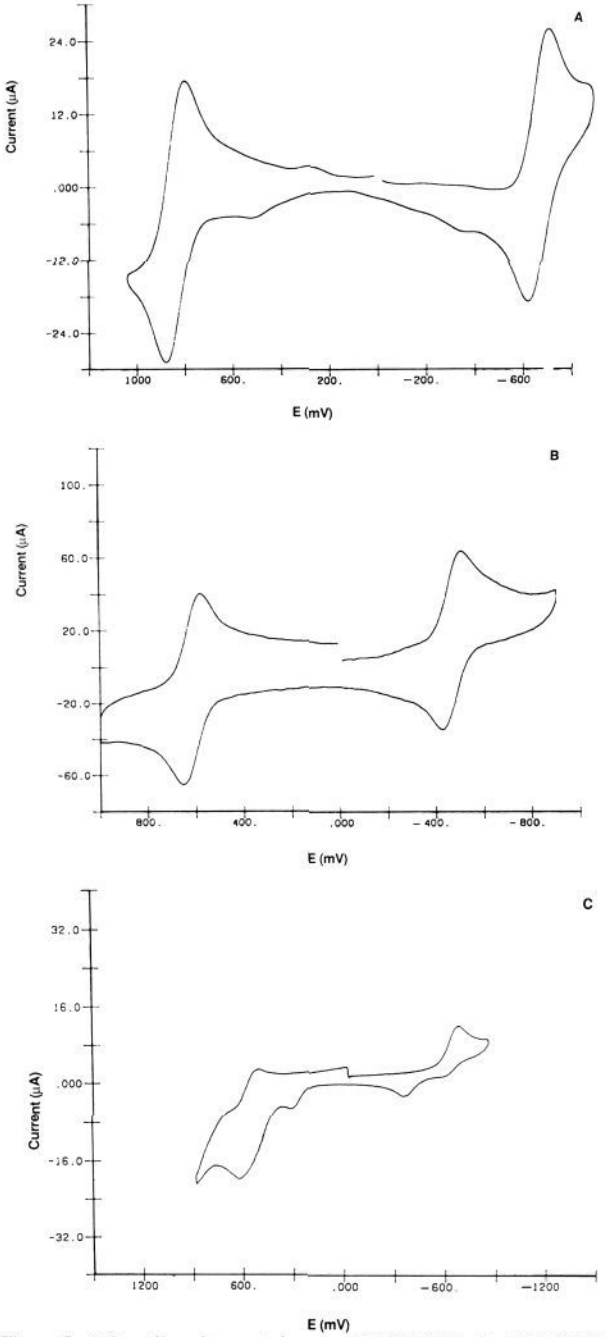

Figure 5. (A) cyclic voltammetric scan of $[Cl(Pic)_4Tc–O–TcCl_4(Pic)]$ in 0.1 M $(Et_4)ClO_4$ in DMF at room temperature. (B) CV scan of $[Cl(Pic)_3ClTc–O–Tc(Pic)Cl_3(Pic)]$ under the same conditions. (C) CV scan of $[Br(Pyr)_4Tc–O–TcBr_4(Pyr)]$, same conditions as in part A.

ments in the range of 0.9 to 1.3 μ_B, when corrected for the diamagnetic contributions of the ligands. Solid-state EPR signals were severely broadened and barely observable at room temperature and were broad but easily observable at −170 °C. EPR spectra of $[Cl(Pic)_4Tc–O–TcCl_4(Pic)]$ taken in frozen chloroform solutions at −170 °C, exhibited an extremely complicated signal. Line splitting at the level of resolution obtained can be attributed to an axial signal ($g_\parallel$ = 1.9275 and $g_\perp$ = 1.997) split strongly by the $^9/_2$ spin on one technetium ($a_\parallel$ = 272.3 G and $a_\perp$ = 163.3 G) and less strongly by a second technetium ($a_\parallel'$ = 31.0 G and $a_\perp'$ = 60.1 G). The actual and simulated EPR spectra are shown in Figure 3. As in the ESR spectra of $[(NO)Cl_4Tc^{II}]^-$,[30] additional

(30) Yang, G. C.; Heitzmann, M. W.; Ford, L. A.; Benson, W. R. *Inorg. Chem.* **1982**, *21*, 3242–3243.

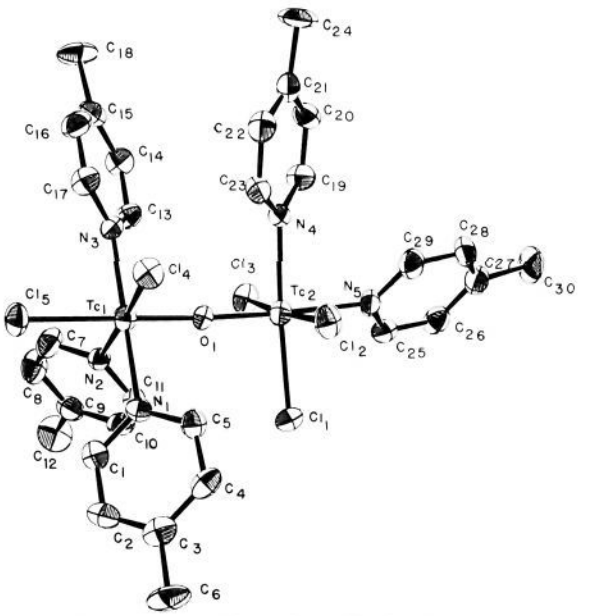

Figure 6. Structure of $[Cl(Pic)_3ClTc–O–Tc(Pic)Cl_3(Pic)]$. Thermal ellipsoids are given at 50% probability for Tc, Cl, O, and N atoms. Carbon atoms are isotropic at 50% probability.

splitting was not observed for the ^{35}Cl and ^{37}Cl nuclei ($I = {}^3/_2$) Cl or ^{14}N (I = 1). The EPR spectrum for III (shown in Figure 4) appears to be rhombic with parameters in the same range as given for I.

Electrochemistry. Formal reduction potentials as determined in 0.1 M $(Et_4N)ClO_4$ in DMF at room temperature are listed in Table VII. In general, peak separations ($\Delta E_{pc,pa}$) were similar to those of the ferrocene internal standard at the same scan rate and approached 59 mV at slow scan rates. Peak heights, essentially identical with equimolar solutions of ferrocene, indicate the couples to involve the transfer of a single electron. As noted in Table VII, the dissymmetric complexes with bromo ligands tended to show irreversible CV waves corresponding to the reduction of the mixed-valence complexes. Consistent with this, a number of complexes exhibited new waves following reduction of the mixed-valence form, indicating at least partial transformation of the complex following reduction.

Cyclic voltammetry of the picoline–chloro compounds in DMF revealed two nearly reversible (on the CV time scale) electron-transfer processes (see Figure 5A); however, irreversible chemical change was immediately evident in acetonitrile. Plots of i_p versus $v^{1/2}$ for I were approximately linear up to a scan rate of 350 mV/s, indicating the couples to be both chemically and electrochemically reversible at relatively fast scan rates. However, subsequent scans revealed new current peaks to grow in around 0.47 V and −0.38 V. The former couple also fulfilled the criteria for chemically and electrochemically reversible couples on the CV time scale. The asymmetric complexes were usually more stable than the corresponding dissymmetric species following electron transfer (see Figure 5B and Table VII).

The dissymmetric bromo complexes showed somewhat more variation in their electrochemistry and all exhibited irreversible cathodic reduction waves (Figure 5C). The pyridine and picoline complexes also showed new couples around −0.2 V, which were often present even on the first scan and whose current increased with subsequent scans.

Structure Descriptions. The structure of III is shown in Figure 6 and that for I is given in Figure 7. Table VIII contains the atomic coordinates of the atoms in the asymmetric unit. The bond distances and angles surrounding the essentially octahedral technetium atoms are listed in Tables IX and X, respectively. The geometry is essentially octahedral around each Tc, which are linked by a μ-oxo bridge, with the equatorial ligands on each Tc being staggered relative to those on the other. The Tc–O, Tc–N, and

Table VIII. Atomic Coordinates in the Unit Cell of $[Cl(Pic)_3ClTc-O-Tc(Pic)Cl_3(Pic)]$

atom type	coordinates[a] x	y	z
Tc1	7002 (1)	2287 (1)	8487 (1)
Tc2	4437 (1)	3073 (1)	9068 (1)
O1	5731 (2)	2700 (2)	8752 (1)
Cl1	4924 (1)	4539 (1)	8962 (1)
Cl2	3561 (1)	3105 (1)	7914 (1)
Cl3	3796 (1)	1647 (1)	9284 (1)
Cl4	8034 (1)	3535 (1)	8900 (1)
Cl5	8663 (1)	1664 (1)	8127 (1)
N1	6737 (3)	2908 (3)	7472 (2)
N2	6182 (3)	1166 (3)	8068 (2)
N3	7275 (3)	1666 (3)	9504 (2)
N4	5152 (3)	3092 (3)	10138 (2)
N5	2931 (3)	3512 (3)	9501 (3)
C1	7002 (4)	2539 (3)	6851 (3)
C2	6858 (4)	2957 (4)	6199 (3)
C3	6413 (4)	3779 (4)	6157 (3)
C4	6102 (4)	4133 (4)	6801 (3)
C5	6283 (4)	3695 (3)	7437 (3)
C6	6294 (5)	4248 (4)	5445 (3)
C7	6588 (4)	363 (4)	8140 (3)
C8	6063 (5)	-364 (3)	7888 (3)
C9	5039 (5)	-303 (4)	7540 (3)
C10	4629 (4)	530 (4)	7476 (3)
C11	5197 (4)	1232 (3)	7735 (3)
C12	4428 (5)	-1106 (4)	7252 (3)
C13	6511 (4)	1173 (3)	9777 (3)
C14	6648 (4)	753 (4)	10418 (3)
C15	7612 (5)	817 (4)	10825 (3)
C16	8384 (4)	1351 (4)	10541 (3)
C17	8206 (4)	1752 (4)	9894 (3)
C18	7837 (5)	303 (4)	11520 (3)
C19	4636 (4)	2832 (4)	10704 (3)
C20	5033 (4)	2945 (4)	11394 (3)
C21	6027 (5)	3322 (4)	11547 (3)
C22	6579 (4)	3549 (4)	10947 (3)
C23	6140 (4)	3436 (3)	10263 (3)
C24	6465 (5)	3519 (4)	12304 (3)
C25	1984 (4)	3141 (4)	9302 (3)
C26	1029 (4)	3331 (4)	9625 (3)
C27	1012 (5)	3905 (4)	10180 (3)
C28	1972 (5)	4303 (4)	10363 (3)
C29	2912 (5)	4109 (3)	10022 (3)
C30	11 (5)	4069 (4)	10581 (3)

[a] The numbers in parentheses are the estimated standard deviations.

Table IX. Bond Distances in the Technetium Coordination Spheres of $[Cl(Pic)_3ClTcOTc(Pic)Cl_3(Pic)]$

bond type	distance, Å	bond type	distance, Å	bond type	distance, Å
Tc1-O1	1.800 (3)	Tc1-N1	2.142 (4)	Tc1-N2	2.139 (4)
Tc1-N3	2.147 (4)	Tc1-Cl4	2.421 (2)	Tc1-Cl5	2.407 (2)
Tc2-O1	1.837 (3)	Tc2-N4	2.150 (4)	Tc2-N5	2.188 (4)
Tc2-Cl1	2.357 (2)	Tc2-Cl2	2.370 (2)	Tc2-Cl3	2.389 (2)

[a] The numbers in parentheses are the estimated standard deviations.

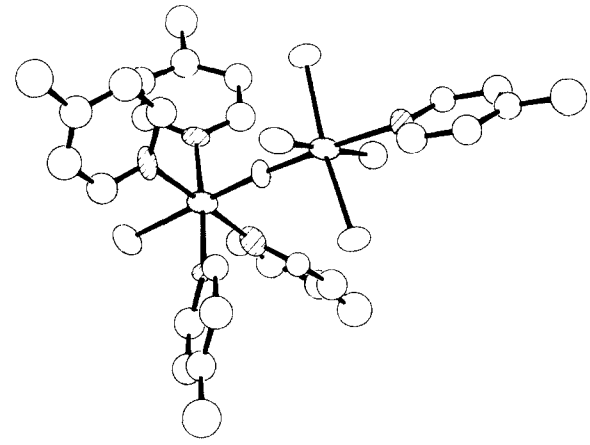

Figure 7. ORTEP diagram of $[Cl(Pic)_4Tc-O-TcCl_4(Pic)]$. Thermal ellipsoids are given at 50% probability for Tc, Cl, O, and N atoms. Carbon atoms are isotropic at 50% probability.

Tc–Cl bond distances are comparable to similar distances in related structures with the deviations being dominated by steric effects due to nonbonded contacts.[1,3,6]

While in compound I the two Tc–O bond distances (1.80 (1) and 1.83 (1) Å) are not different on a 2σ basis,[9] in compound III the Tc1–O distance of 1.800 (3) Å is clearly shorter than the Tc2–O distance (1.837 (3) Å), Tc1 having two chlorines and three nitrogens and Tc2 having two nitrogens and three chlorines. Contrary to expectations, if oxidation states are assigned in a conventional fashion, the Tc–O distance for Tc1(III) is shorter than that for Tc2(IV). This is possibly due to the steric effect exerted on the bridging oxygen by the 3 or 4 equatorial chlorines, which exhibit O···Cl contact distances of 3.05 to 3.11 Å.

The average equatorial Tc–N distances of 2.15 (2) Å in compound I and 2.143 (3) Å in compound III are similar to those found in other complexes with $[O{=}Tc{=}O]^+$ cores.[6] The slightly longer axial Tc–N distances of 2.20 (2) Å in compound I and 2.188 (4) Å in compound III can be attributed to a trans effect exerted by the μ-O. The average axial and equatorial Tc–Cl distances in compound I are 2.39 (1) and 2.37 (1) Å, respectively. Similarly, in compound III the axial Tc2–N5 distance is 2.407 (2) Å and the average equatorial Tc2–Cl distance is 2.37 (2) Å; however, the equatorial Tc1–Cl4 distance is the longest in the structure at 2.421 (2) Å. In six coordinate technetium Tc(II) through Tc(V) complexes with a chloride trans to a chloride or singly bonded nitrogen, the "average" Tc–Cl bond distance is 2.34 Å[3]. The "average" Tc–Cl distance increases to 2.43 Å if the chlorine is trans to a π-acid such as phosphorus, or 2.44 Å in eight coordinate species. In compound III the Tc1–Cl4 bond distance is 0.05 Å longer than the average of the other equatorial Tc–Cl distances or 0.08 Å longer than the "average" Tc–Cl distance. A trans effect due to the picoline seems unlikely, and the Tc2-Cl2 bond distance (trans to N4) is not elongated (2.370 (2) Å).

Table X. Bond Angles in the Technetium Coordination Spheres of $[Cl(Pic)_3ClTcOTc(Pic)Cl_3(Pic)]$

bond type	angle, deg	bond type	angle, deg	bond type	angle, deg
O1-Tc1-N1	89.6 (1)	O1-Tc1-N2	89.0 (1)	O1-Tc1-N3	90.6 (1)
O1-Tc1-Cl4	94.9 (1)	O1-Tc1-Cl5	177.2 (1)	N1-Tc1-N2	89.5 (1)
N1-Tc1-N3	179.8 (1)	N2-Tc1-N3	90.7 (1)	N1-Tc1-Cl4	88.8 (1)
N1-Tc1-Cl5	91.3 (1)	N2-Tc1-Cl4	175.8 (1)	N2-Tc1-Cl5	88.4 (1)
N3-Tc1-Cl4	91.0 (1)	N3-Tc1-Cl5	88.5 (1)	Cl5-Tc1-Cl4	87.82 (5)
O1-Tc2-N4	89.0 (1)	O1-Tc2-N5	177.0 (1)	O1-Tc2-Cl1	92.4 (1)
O1-Tc2-Cl2	94.4 (1)	O1-Tc2-Cl3	94.0 (1)	N4-Tc2-N5	88.1 (1)
N4-Tc2-Cl1	88.4 (1)	N4-Tc2-Cl2	176.5 (1)	N4-Tc2-Cl3	88.8 (1)
N5-Tc2-Cl1	87.1 (1)	N5-Tc2-Cl2	88.6 (1)	N5-Tc2-Cl3	85.6 (1)
Cl1-Tc2-Cl2	90.58 (5)	Cl1-Tc2-Cl3	172.90 (5)	Cl2-Tc2-Cl3	91.92 (5)
Tc1-O1-Tc2	176.5 (2)	C1-N1-Tc1	122.9 (3)	C5-N1-Tc1	119.5 (3)
C7-N2-Tc1	123.0 (3)	C11-N2-Tc1	120.8 (3)	C13-N3-Tc1	120.9 (3)
C17-N3-Tc1	122.0 (3)	C19-N4-Tc2	123.2 (3)	C23-N4-Tc2	119.6 (3)
C25-N5-Tc2	121.2 (3)	C29-N5-Tc2	122.1 (4)	C1-N1-C5	117.6 (4)

[a] The numbers in parentheses are the estimated standard deviations in the last significant figure.

Nonbonded steric effects provide a reasonable explanation for this. In particular, the close approach of the α-carbons on a picoline cis to the chlorine may be the dominant factor. The picoline rings are tilted with respect to the equatorial mean plane by 37–55° and the equatorial ligands on opposing technetiums are staggered by 25–37° and not 45°. In compound I, these factors have the effect of placing the α-carbon nearly midway between two chlorines on the opposite technetium.[9] The close α-C···Cl contacts are from 3.27 to 3.53 Å. The sum of van der Waals radii for carbon and chlorine atoms is 3.4–3.5 Å (neglecting the projecting hydrogen atoms). Nonbonded contact of α-carbons on picoline ligands cis to a chlorine can be noted in the structure of the Tc(II)–Tc(III) dimer of α-pyridone, $[Tc_2(OC_5H_4N)_4]Cl$, in which the pyridone ligand bridges the Tc–Tc unit, locking the pyridine ring perpendicular to the mean plane of the equatorial ligands, thus prohibiting a closer approach of the chlorine and the $[Tc_2(OC_5H_4N)_4]$ units are linked by a bridging chlorine with a long Tc–Cl distance of 2.678 Å.[31] On the basis of the reported coordinates for this compound the Cl···C5 (C5 is the α-carbon on the pyridone) contact distance is 3.28 Å.

Tissue Distribution. The distributions of *trans*-$[O_2(Pic)_4Tc]^+$, $[Cl(Pic)_3ClTc–O–Tc(Pic)Cl_3(Pic)]$, and $[Cl(Pic)_4Tc–O–Tc(Pic)Cl_4]$ in selected mouse tissues are illustrated in the supplementary material.

Discussion

Synthesis. Since these compounds are so readily prepared from technetium starting materials in the IV, V, or VII oxidation states, it appears that this type of complex is thermodynamically favored in neat pyridine solutions. Their ion-exchange behavior, rapid solubility and nonconductivity in low-dielectric, aprotic solvents, and the lack of a counterion in the crystal structure are consistent with their being formulated as neutral species. The lack of a mirror plane of symmetry (σ_h) in these molecules is highly unusual, if not unique, for spontaneously generated μ-oxo species, and it is likely that the dark, crystalline-like materials noted by previous workers[8] on allowing *trans*-$[O_2(Pyr)_4Tc]^+$ to stand in neat pyridine for extended periods are composed of the types of compounds reported here.

Plots of the various products as a function of time (Figure 1) suggest the asymmetric species to be precursors of the dissymmetric complexes, since the concentration of the asymmetric complexes rises and falls as expected for a kinetic intermediate and a simple linkage isomerization reaction can be conceived to result in the dissymmetric product. Similarly, mass balance considerations indicate that technetium involved in III must be converted to that in I. Conversely, these plots imply that *trans*-$[O_2(Pyr)_4Tc]^+$ may not be a precursor of the μ-oxo complexes, since its concentration does not drop off rapidly as the reaction proceeds and condensation with a species such as $[OCl_4Tc]^-$ would directly yield a dissymmetric product.

While $[O_2(Pyr)_4Tc]^+$ does not appear to be a precursor to the dimeric complexes, its appearance in the reaction media suggests the equilibria illustrated in Scheme I to be occurring. Indeed, complexes of the general type containing two pyridine and two halide ligands have already been described.[7] Since the formation of these compounds most likely involves the condensation of two different technetium complexes in an asymmetric fashion, a reaction involving the asymmetric monomers shown in Scheme I may be occurring. While no direct evidence was gathered on the mode of technetium reduction, the pyridine solvent is the most likely source of electrons and this may occur by oxygen atom transfer.

Spectra and Electrochemistry. The infrared spectra of these complexes are similar to those of other μ-oxo species but the assymetric Tc–O–Tc stretching frequencies appear at somewhat lower energy than for μ-oxo-rhenium(V) species.[32] On the other hand, the ν_{assym} occur at slightly higher energy than observed in μ-O-$[O(Et_2dtc)_2Tc]_2$, which is consistent with the absence of axial oxo ligands and equatorial sulfur ligands[33] that should tend to weaken the π-bonding between the metal and the bridging oxygen.

Scheme I. Equilibria Involving Various Pyridine and Halide Ligands in Tc(V) Di- and Mono-oxo Complexes

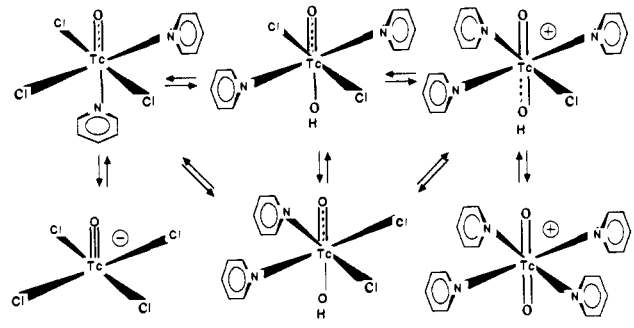

The absorptions at 250–260 nm in the electronic spectra of all the complexes probably arise from π–π* transitions on the pyridine ligands. Since the bands around 350–380 nm vary with the halide present, it is likely that these are due to halide-to-technetium charge-transfer transitions. The other bands above 290 nm are unassigned but may derive from pyridine-to-technetium charge-transfer transitions.

The NIR bands listed in Table IV occur in a region expected for (what are still termed) IVCT bands in strongly coupled mixed-valent compounds.[23] While most mixed-valent compounds exhibit only a single IVCT transition, the appearance of as many as three bands has been attributed to a strong tetragonal distortion in the ligand field[34] and to spin–orbit coupling.[35] Owing to the μ-oxo bridge, such distortion seems likely for these complexes. The bandwidths listed in Table V are only one-fourth to one-third as large as predicted by the relation: $\Delta\nu_{1/2} = [2310(\nu_{max} - \Delta E)]^{1/2}$, which applies when the metal ions are moderately coupled. (The ESCA data suggest that ΔE, the difference in ground-state electronic energies between the metal centers, is relatively small.) However, such narrow bandwidths are fully consistent with strongly coupled mixed-valent complexes.[23]

The electrochemical measurements indicate that these complexes can be oxidized or reduced by a single electron. While many of these couples appear to be nearly chemically reversible on the relatively rapid cyclic voltammetric time scale in nonaqueous media, subsequent chemical changes take place fairly quickly to produce species that are usually more easily oxidized and reduced. It is likely that the lower oxidation states are partially stabilized by the pyridine ligands and that most of the added electron density is concentrated on the technetium equatorially coordinated by the large number of pyridines, since these would be able to absorb some of the additional charge density through π–d_π back-bonding. This suggests that these complexes may be useful in the synthesis of low-valent technetium complexes stabilized by pyridine or other π-acceptor ligands.

The mean comproportionation constants (K_{COM})[36] for the chloro complexes calculated from electrochemical data listed in Table VII are 1.3×10^{26} for the dissymetric compounds and 3.4×10^{19} for the asymmetric compounds. These values are so large as to indicate a resonance (strongly coupled, Robin & Day class III)

(31) Cotton, F. A.; Fanwick, P. E.; Gage, L. R. *J. Am. Chem. Soc.* **1980**, *102*, 1570–1577.

(32) Jezowska-Trzebiatowska, B.; Hanuza, J. *J. Mol. Struc.* **1973**, *19*, 109–142.

(33) Thomas, R. W.; Davison, A.; Trop, H. S.; Deutsch, E. *Inorg. Chem.* **1980**, *19*, 2840.

(34) Joss, S.; Reust, H.; Ludi, A. *J. Am. Chem. Soc.* **1981**, *103*, 981.

(35) Kober, E. M.; Goldsby, K. A.; Narayana, D. N. S.; Meyer, T. J. *J. Am. Chem. Soc.* **1983**, *105*, 4303–4309.

(36) Comproportionation is the reaction of a higher and lower oxidation state of the same complex to give an intermediate state. For compound I, this would be $[I]^+ + [I]^- \rightarrow 2\,[I]$. The tendency for this reaction to occur indicates the degree of delocalization of the unpaired electron in the intermediate oxidation state.

or, at least, intermediately delocalized setting (Robin & Day class II).[37] While a correction must be made for the lack of symmetry in these complexes, the difference between these two types of compounds suggests the "corrected" comproportionation constant to be in the range of 10^9–10^{10}.[38]

Structure. Aside from their low symmetry, the structures of these compounds are similar to those commonly observed for μ-oxo complexes in that the average Tc–O bond distance of 1.82 Å is significantly shorter than that observed for a Tc–O single bond (2.02 Å)[39] and the metal–oxygen–metal moiety is essentially linear.[40] These characteristics indicate significant π-bonding between the technetium atoms and the oxygen, presumably involving the donation of electron pairs in the oxygen p_x and p_y orbitals of the oxygen to d_π orbitals on the metal ions.[41,42] Since the Tc–O–Tc moiety is nearly linear and exhibits evidence of being partially π-bonded, it is improbable that the bridge involves hydroxide. Hydroxo-bridged species are usually strongly bent and exhibit M–O bond distances similar to those of single bonds.[3,43] The Tc–N and Tc–Cl bond distances are well within the range observed in a variety of other technetium complexes[1,3,6] with the μ-oxo exhibiting a small trans influence on the axial ligands. Steric hindrance forces the picoline and chloride ligands to adopt a staggered configuration and pushes the plane of the equatorial chlorides back from Tc1 (or Tc3) in I by 0.1 Å. The staggered arrangement and the substantial distance (3.64 Å) between the two technetiums precludes significant metal–metal bonding in either type of complex. While crystallizing in a similar space group, the asymmetric complex with an effective volume of 900 $Å^3$/molecule packs somewhat more efficiently than the dissymetric complex (989.8 $Å^3$/molecule).

Magnetic Properties. Since technetium has seven valence electrons, a 7^+ charge distributed over two atoms requires that there also be seven d electrons in the molecule. In a magnetically dilute solid these odd-electron compounds should yield a significant magnetic moment; however, the fairly small values of μ_{eff} observed indicate the presence of only one unpaired electron strongly affected by spin–orbit coupling. While antiferromagnetic coupling between molecules might also be invoked to account for the low μ_{eff}, in the crystal structure of I the closest contact between adjacent molecules is 3.5 Å and this involves only a minor overlap between parallel pyridine rings. This makes antiferromagnetic coupling, of the strength necessary to account for the observed effects, highly unlikely.

The solid-state EPR spectra and highly shifted and broadened ^1H NMR signals verify that these compounds are paramagnetic. The frozen solution EPR spectra of I was reasonably well simulated (Figure 3) by assuming a single electron with substantial spin density on one metal ion, but with significant distribution onto the second. The clear axial symmetry of the frozen solution spectra of I and the low magnetic susceptibilities imply strong spin–orbit coupling. This indicates that the single unpaired electron resides in a π-orbital involving both technetiums and the bridging oxygen. Assuming participation of the d_{xz} and d_{yz} orbitals on separate metal ions and the p_x and p_y orbitals on the oxygen, the orbital angular momentum may result from the electron's being able to move between nearly degenerate π-orbitals and thereby circulate around the z axis. By analogy to molecular orbital descriptions given for other, linear, second-row, μ-oxo compounds,[44-46] the unpaired electron should be located in a nonbonding or weakly antibonding π-molecular orbital involving a p orbital on the oxygen and a d_π orbital on each Tc. This bonding scheme also accounts for the existence of only one unpaired electron, since the axial distortion imposed by the π-bonding should significantly lower the relative energy of the d_{xy} orbitals on the two technetiums so that these each contain paired electrons. Substantial π-bonding or strong antiferromagnetic coupling accounts for the pairing of the remaining Tc 4d electrons. Owing to the large number of variable parameters, the EPR spectrum for III could only be approximately simulated. However, these simulations yielded parameters similar to those for I and were consistent with a rhombic spectrum, as would be expected for an asymmetric paramagnetic compound.

Photoelectron Spectra. Symmetric μ-oxo mixed-valence compounds usually show no measurable difference in the ESCA spectra of the two metal ions.[40] However, the preponderance of chlorides around one Tc, and pyridine ligands around the other, in both types of μ-oxo technetium complexes is suggestive of significantly different oxidation states within each complex, but these cannot be assigned unequivocally. Given the 7+ charge that must be distributed between the two technetiums, the nature of their coordination spheres, and the nearly invariant ESCA average binding energy of 254.6 ± 0.2 eV, it seems likely that both are in a mid-oxidation state, i.e., between Tc(II) and Tc(V). This leads to probable formulations of the binuclear species as either $[Tc^{II}–Tc^{V}]$ or $[Tc^{III}–Tc^{IV}]$, with the ion in the lower oxidation state probably coordinating the greater number of pyridine ligands. While comparison of this binding energy with those for technetium ions with well-defined oxidation states would place the technetiums in these compounds in the range of Tc(II) complexes,[47] their total oxidation state and near equivalence compels a higher value. Nevertheless, this suggests that the metal ions have a fairly high degree of electron density, which may be due to π-bonding from the ligands. The lower ionization energy of the μ-oxygen atoms in the chloro compounds compared to $[TcO_4]^-$[25] suggests an increase in electron density on this oxygen relative to other oxotechnetium species, and the further slight decrease in the bromo analogues is in keeping with the expected increase in π-donation in descending the halogen series. This suggests that the π-electron density on the μ-O may be modulated by the halide ligands and mediated by one or both technetiums.

The nearly identical technetium ionization energies cannot be taken to imply that the technetiums share the same oxidation state, since the charge on the metal can vary substantially for a given oxidation state and there is significant overlap in ionization potentials between technetium oxidation states.[26,47] Nevertheless, it is likely that the oxidation states of the two technetiums are within a single unit and may be assigned either as Tc(III)–Tc(IV), with the higher oxidation state coordinating the greater number of halides, or Tc(3.5)–Tc(3.5). Given the equal charge on both technetiums, the difference in Tc–μ–O bond distances may be attributed to the Tc with fewer chlorides accepting more π-electron density from the μ-oxo via a π-bond, so yielding a shorter bond length.

Tissue Distributions. The relatively high liver uptake noted for both compounds is expected for lipophilic molecules, which are often extracted by the liver. The localization of these compounds in the lung and the large variation in this quantity may be due to their low solubility in water, causing varying levels of colloidal precipitation when the injected water/ethanol solutions mix with the venous blood. In the case of *trans*-$[O_2(Pic)_4Tc]^+$, hydrolysis of the picoline ligands with subsequent formation of bridged μ-hydroxo compounds or $TcO_2 \cdot nH_2O$ may also yield colloids. After being pumped through the heart, the blood proceeds to the lungs, where large colloidal particles can become lodged in alveolar

(37) Robin, M. B.; Day, P. *Adv. Inorg. Chem. Radiochem.* **1967**, *10*, 247.
(38) The correction is estimated by extrapolating the 6.5 order of magnitude difference between the dissymmetric and asymmetric complexes to the "symmetric" case, where each Tc has 2.5 pyridine and 2.5 chloro ligands.
(39) Bandoli, G.; Mazzi, U.; Roncari, E.; Deutsch, E. *Coord. Chem. Rev.* **1982**, *44*, 191–227.
(40) Hanuza, J.; Baluka, M.; Jezowska-Trzebiatowska *Acta Phys. Pol.* **1972**, *A42*, 537–551.
(41) Use of a modification of Pauling's bond-order relation (see following reference) with standard average Tc–O bond lengths (Tc—O, 2.02 Å, Tc═O, 1.75 Å, and Tc═O, 1.65 Å) yields a Tc—O bond order of 1.67.
(42) Pauling, L. *The Nature of the Chemical Bond*, 3rd ed.; Cornell University Press: Ithaca, NY, 1960; p 239.
(43) Libson, K.; Deutsch, E.; Barnett, B. L. *J. Am. Chem. Soc.* **1980**, *102*, 2477–2478.
(44) Dunitz, J. D.; Orgel, L. E. *J. Chem. Soc.* **1953**, 2594.
(45) Weaver, T. R.; Meyer, T. J.; Adeyemi, S. A.; Brown, G. M.; Eckberg, R. P.; Hatfield, W. E.; Johnson, E. C.; Murray, R. W.; Untereker, D. *J. Am. Chem. Soc.* **1975**, *97*, 3039–3046.
(46) Griffith, W. P. *Coord. Chem. Rev.* **1970**, *5*, 459–517.
(47) Gerasimov, V. N.; Kryuchkov, S. V.; Kuzina, A. F.; Kulakov, V. M.; Pirozhkov, S. V.; Spitsyn, V. I. *Dokl. Akad. Nauk USSR* **1982**, *266*, 148.

capillaries.[1] Since the reticuloendothelial systems of the liver and spleen also extract smaller colloids, some of the uptake exhibited by these two organs may be due to colloid formation in the blood. However, the moderate spleen uptake suggests that this is not responsible for the substantial localization of these compounds in the liver.

Even though the complexes are neutral, they did not efficiently cross the blood–brain barrier (although the presence of ethanol may have affected this) and so would need substantial modification to be developed as candidates for brain-imaging agents. On the other hand, the heart uptake exhibited by I was unexpected and derivatives that would cause this uptake to be accumulative might prove useful. Since these compounds are presently efficiently prepared only with millimolar concentrations of technetium, they cannot now be easily derived from the no-carrier-added ^{99m}Tc solutions normally used in radiopharmaceutical synthesis, which are typically in the nano- to micromolar range. Nevertheless, a better understanding of the mechanism of formation of these complexes may yield reactions capable of synthesizing these types of complexes at low technetium concentration.

Conclusion. These complexes are unusual examples of unsymmetrical, mixed-valent complexes in which the unpaired electron is delocalized[22] and in which strong tetragonal distortion is evident in the IVCT bands. The high solubility of these complexes in low dielectric solvents, their adherence to Beer's law, their small solution conductivities, their failure to be immediately retained by ion exchange columns, and clear evidence for binuclear species in the solution EPR spectra provide convincing evidence that these compounds are essentially identical in both solution and the solid state. The presence of only monodentate ligands and the ability to undergo electron transfer suggest these complexes as a synthetic route to lower technetium oxidation states. This is especially attractive since the main obstacle to obtaining these species—elimination of multiply bonded oxygen—has been overcome. Finally, the ability to easily prepare both asymmetric and dissymmetric technetium complexes with heterocyclic ligands opens synthetic avenues for the preparation of technetium complexes which can bind to biologically important molecules such as nucleotides, coenzymes, and nucleic acids. Indeed, their tendency to slowly and irreversibly bind to ion exchange materials suggests that they may be able to firmly attach to charged biopolymers, such as nucleic acids.

Acknowledgment. This work was supported by PHS Grant GM26390. ESR spectra and helpful discussions on their interpretation were provided by Drs. Hans Van Willigen and T. K. Chakesandra at the University of Massachusetts (Boston). Dr. Jack Spence of Utah State University generously provided the VAX version of EPROW and Dr. Dennis Chasteen of the University of New Hampshire guided us in its use. We are also grateful to Prof. Harvey Shugar at Rutgers University for collecting the crystallographic data set.

Registry No. I, 112816-10-1; II, 112816-18-9; III, 112816-15-6; $[Cl(Pyr)_4TcOTcCl_4(Pyr)]$, 112816-08-7; $[Br(Pyr)_4TcOTcBr_4(Pyr)]$, 112816-09-8; $[Br(Pic)_4Tc{\cdot}OTcBr_4(Pic)]$, 112816-11-2; $[Cl(Lut)_4TcOTcCl_4(Lut)]$, 112816-12-3; $[Cl(Pyr)_3ClTcOTc(Pyr)Cl_3(Pyr)]$, 112816-13-4; $[Br(Pyr)_3BrTcOTc(Pyr)Br_3(Pyr)]$, 112816-14-5; $[Br(Pic)_3BrTcOTc(Pic)Br_3(Pic)]$, 112816-16-7; $[Cl(Lut)_3ClTcOTc(Lut)Cl_3(Lut)]$, 112816-17-8; $[(n\text{-}Bu)_4N][TcOCl_4]$, 92622-25-8; $[(n\text{-}Bu)_4N][TcOBr_4]$, 92622-23-6; $[(n\text{-}Bu)_4][TcCl_6]$, 112816-19-0; $[(n\text{-}Bu)_4N][TcBr_6]$, 112816-20-3; $(NH_4)TcO_4$, 34035-97-7; $[(n\text{-}C_4H_9)_4N][TcO_4]$, 111127-64-1.

Supplementary Material Available: Tables of temperature factors for non-hydrogen atoms, bond distances and angles for picoline ligands, electronic spectra for $[Cl(Pic)_4Tc\text{–}O\text{–}TcCl_4(Pic)]$ in various solvents, complete listings of infrared, figures showing closest contacts of picoline rings in I, solid state and room temperature EPR spectra, and figures of UV–visible spectra and biological tissue distributions (24 pages); listing of calculated and observed structure factor amplitudes for $[(Pic)Cl_3(Pic)Tc\text{–}O\text{–}TcCl(Pic)_3Cl]$ and $[Cl(Pic)_4Tc\text{–}O\text{–}TcCl_4(Pic)]$ (64 pages). Ordering information given on any current masthead page.

Cobalt and Manganese Complexes of a Schiff Base Biquinone Radical Ligand

Scott K. Larsen and Cortlandt G. Pierpont*

Contribution from the Department of Chemistry and Biochemistry, University of Colorado, Boulder, Colorado 80309. *Received July 7, 1987*

Abstract: Reactions between 3,5-di-*tert*-butylcatechol, aqueous ammonia, and divalent metal ions produce neutral complexes containing a tridentate ligand formed by the Schiff base condensation of two catechol molecules with NH_3. The free ligand may exist in electronic forms ranging in charge from +1 to −3, and, in complexes formed with divalent metal ions that are not electroactive, the ligand bonds in the −1 form, $M^{II}(Cat\text{-}N\text{-}BQ)_2$. With electroactive metal ions a charge balance is reached between metal and ligands by intramolecular electron transfer. The complex prepared with Mn(II) shows structural features that are consistent with a complex containing Mn(IV) with ligands in the radical dianion Cat-N-SQ form, $Mn^{IV}(Cat\text{-}N\text{-}SQ)_2$. The complex contains one unpaired electron due to coupling between the two radical ligands and the d^3 metal ion. Isotropic and anisotropic EPR spectra verify that the unpaired electron resides in a metal-localized orbital. Electrochemistry shows redox activity for both metal and ligands and the electronic spectrum of the complex shows four intense bands in the near-infrared. The related complex prepared with Co(II) shows structural features of Co(III), requiring one ligand in the −1 form and the second in the form of the −2 radical, $Co^{III}(Cat\text{-}N\text{-}BQ)(Cat\text{-}N\text{-}SQ)$. This molecule also contains a single unpaired electron, but with the diamagnetic metal ion, the electron is in a ligand-localized orbital. The EPR spectrum verifies this, but shows an unusually simple hyperfine pattern consisting of 16 lines due to coupling to the $I = {}^7/_2$ metal and one $I = {}^1/_2$ center, presumably one ligand proton. This result appears to indicate that the unpaired electron is regionally localized on one ligand on the EPR time scale.

Studies on the coordination of semiquinonate and catecholate ligands to transition-metal ions have shown that the intramolecular charge distribution between metal and quinone is sensitive to several effects. The increase in orbital energy on the metal for third-row metals relative to metals of the first transition series results in catecholate complexes of hexavalent metal ions, M^{VI}-

0002-7863/88/1510-1827$01.50/0